# Virological response to nucleos(t)ide analogues treatment in chronic hepatitis B patients is associated with *Bacteroides*-dominant gut microbiome

Saisai Zhang,[a,f] Hau-Tak Chau,[a,f] Hein Min Tun,[b,c] Fung-Yu Huang,[a] Danny Ka-Ho Wong,[a,d] Lung-Yi Mak,[a,d] Man-Fung Yuen,[a,d,**] and Wai-Kay Seto[a,d,e,*]

[a]Department of Medicine, School of Clinical Medicine, The University of Hong Kong, Hong Kong, China
[b]The Jockey Club School of Public Health and Primary Care, Faculty of Medicine, The Chinese University of Hong Kong, Hong Kong, China
[c]System Microbiology and Antimicrobial Resistance (SMART) Lab, Li Ka Shing Institute of Health Sciences, The Chinese University of Hong Kong, Hong Kong, China
[d]State Key Laboratory of Liver Research, The University of Hong Kong, Hong Kong, China
[e]Department of Medicine, The University of Hong Kong-Shenzhen Hospital, Shenzhen, China

eBioMedicine
2024;103: 105101
Published Online xxx
https://doi.org/10.1016/j.ebiom.2024.105101

## Summary

**Background** Gut dysbiosis is present in chronic hepatitis B virus (HBV) infection. In this study, we integrated microbiome and metabolome analysis to investigate the role of gut microbiome in virological response to nucleos(t)ide analogues (NAs) treatment.

**Methods** Chronic HBV patients were prospectively recruited for steatosis and fibrosis assessments via liver elastography, with full-length 16S sequencing performed to identify the compositional gut microbiota differences. Fasting plasma bile acids were quantified by liquid chromatography-tandem mass spectrometry.

**Findings** All patients (n = 110) were characterized into three distinct microbial clusters by their dominant genus: c-*Bacteroides*, c-*Blautia*, and c-*Prevotella*. Patients with c-*Bacteroides* had a higher plasma ursodeoxycholic acids (UDCA) level and an increase in 7-alpha-hydroxysteroid dehydrogenase (secondary bile acid biotransformation) than other clusters. In NAs-treated patients (n = 84), c-*Bacteroides* was associated with higher odds of plasma HBV-DNA undetectability when compared with non-c-*Bacteroides* clusters (OR 3.49, 95% CI 1.43–8.96, p = 0.01). c-*Blautia* was positively associated with advanced fibrosis (OR 2.74, 95% CI 1.09–7.31, p = 0.04). No such associations were found in treatment-naïve patients. Increased *Escherichia coli* relative abundance (0.21% vs. 0.03%, p = 0.035) was found in on-treatment patients (median treatment duration 98.1 months) with advanced fibrosis despite HBV DNA undetectability. An enrichment in L-tryptophan biosynthesis was observed in patients with advanced fibrosis, which exhibited a positive correlation with *Escherichia coli*.

**Interpretation** Collectively, unique bacterial signatures, including c-*Bacteroides* and *c-Blautia*, were associated with virological undetectability and fibrosis evolution during NAs therapy in chronic HBV, setting up intriguing possibilities in optimizing HBV treatment.

**Funding** This study was supported by the Guangdong Natural Science Fund (2019A1515012003).



**Keywords:** HBV; Fibrosis; Microbiota; Bile acid; *Bacteroides*

## Introduction

Gut microbiota dysbiosis, known as a compositional and functional alteration in the gut microbiota, is emerging as an influential factor implicated in the clinical course of different chronic liver diseases, including non-alcoholic fatty liver disease (NAFLD), alcoholic liver

*Corresponding author. Department of Medicine, The University of Hong Kong, Hong Kong, China.
**Corresponding author. Department of Medicine, The University of Hong Kong, Hong Kong, China.
*E-mail addresses:* wkseto@hku.hk (W.-K. Seto), mfyuen@hkucc.hku.hk (M.-F. Yuen).
[f]Co-first authorship with equal contribution.

## Research in context

### Evidence before this study

Chronic hepatitis B (CHB) infection has been associated with dysbiosis, and previous evidence has highlighted the negative correlation between the relative abundance of the *Bacteroidetes* phylum and the severity of hepatitis B virus (HBV)-related cirrhosis. However, it remains uncertain whether the gut microbiota has direct implications for disease progression in CHB patients receiving antiviral therapy.

### Added value of this study

In this study, we identified three microbial clusters among the CHB patients which were dominated by the genus *Bacteroides*, *Blautia*, and *Prevotella* respectively. Patients with the *Bacteroides*-dominant cluster exhibited a higher plasma ursodeoxycholic acids (UDCA) level and an increase in secondary bile acid biotransformation than the other two patient groups. Among nucleos(t)ide analogues-treated patients, the *Bacteroides*-dominant cluster was associated with significantly higher odds of achieving plasma HBV DNA undetectability compared to the non-*Bacteroides* clusters. In contrast, the *Blautia*-dominant cluster was positively associated with advanced fibrosis. Notably, no such associations were observed in treatment-naïve patients. Moreover, advanced fibrosis in on-treatment patients after successful virological control was also linked to microbial alterations (e.g., increased abundance of *Escherichia coli* and its association with L-tryptophan biosynthesis) and bile acid metabolism.

### Implications of all the available evidence

To our knowledge, this is the first study that demonstrates a linkage between *Bacteroides*-dominant cluster and HBV treatment response during nucleos(t)ide analogues therapy, which sets up intriguing possibilities for optimizing HBV treatment.

disease, primary sclerosing cholangitis, and hepatocellular carcinoma.[1–5] Dysbiosis has been reported in chronic hepatitis B (CHB) infection, which affects 296 million individuals worldwide with the prevalence being highest in the Western Pacific region.[6] CHB without antiviral treatment may culminate in progress to life-threatening end-stage chronic liver disease, such as cirrhosis or hepatocellular carcinoma. Patients with hepatitis B virus (HBV)-related cirrhosis have a significantly altered gut microbiota community when compared with non-HBV healthy subjects.[7] The relative abundance of *Bacteroidetes* phylum negatively correlated with cirrhosis severity, while *Enterobacteriaceae* members and *Veillonella* demonstrated a positive correlation with cirrhosis.[7] Reconstitution of the gut microbiota by transplantation of fecal microbiota from healthy donors facilitated hepatitis B e antigen (HBeAg) clearance in patients with persistent HBeAg-positive HBV infection after long-term antiviral therapy.[8] The establishment of the commensal microbiota can be a pre-requisite for the age-related immune clearance of HBV.[9] However, it remains uncertain if gut microbiota has any direct associations with disease progression in CHB patients receiving antiviral therapy.

Bile acids interact with the host liver and the gut microbiome based on different metabolism pathways. Primary bile acids, synthesized from cholesterol by the liver, enter the gastrointestinal tract and are biochemically modified by the gut microbiota into secondary bile acids.[10] Like other gut microbial metabolites in the enterohepatic circulation, a portion of bile acids are then transferred back to the liver via the portal circulation. Bile acid metabolism is involved in the pathogenesis of different chronic liver diseases, especially in NAFLD.[11–13] Since concomitant steatosis is present in 40.8% of CHB patients,[14] it is possible that bile acid metabolism and its associated microbial signatures can impact CHB-related outcomes. There may be a more direct role for the involvement of bile acids in CHB; the bile acid transporter sodium taurocholate cotransporting polypeptide (NTCP) is responsible for viral entry of HBV into hepatocytes,[15] suggesting that bile acids may be involved in HBV infection.

In this study, we aimed to identify compositional differences in gut microbiota among a heterogeneous cohort of CHB patients using full-length 16S rRNA sequencing. We further investigated the role of the gut microbiota-bile acid axis in CHB patients referring to the detectability of plasma HBV DNA and the presence of liver fibrosis. The identification of the potential bacterial signatures and the alteration in bile acid metabolism related to different disease spectrums may discover new non-invasive markers for predicting HBV-related treatment efficacy and disease progression.

## Methods

### Patients

We prospectively recruited consecutive chronic HBV patients from the liver clinics of Queen Mary Hospital, Hong Kong during the period December 2019 and September 2020 who were referred for liver transient elastography assessment. The patients were all HBsAg-positive for at least 6 months and were not coinfected with human immunodeficiency virus (HIV), hepatitis C virus (HCV), or the hepatitis Delta virus (HDV). Patients with other chronic liver diseases, including primary biliary cholangitis, primary sclerosing cholangitis, autoimmune hepatitis, Wilson's disease, history of liver

transplantation, history of hepatocellular carcinoma (HCC), and alcoholism were excluded.

All participants underwent a thorough clinical evaluation, including anthropometric and laboratory assessments at the time of recruitment. Anthropometric measurements included body height, body weight, body mass index (BMI), waist circumference, and hip circumference. Laboratory measurements included liver biochemistry, fasting glucose, and glycosylated hemoglobin (HbA1c).

### Assessments of liver parameters

Liver steatosis and fibrosis were assessed by transient elastography using Fibroscan (Echosens®, Paris, France) during the recruitment. Controlled Attenuation Parameter (CAP) was expressed in dB/m and was only considered reliable with an IQR of <40 dB/m.[16] CAP <248 dB/m was categorized as no steatosis and CAP ≥280 dB/m was categorized as severe steatosis.[17] Liver stiffness measurement was presented as the median value of ≥10 successful acquisitions in kPa. Absent or minimal liver fibrosis (F0/F1), the "grey-zone" and advanced liver fibrosis (F3/F4) were defined as liver stiffness <6 kPa, 6–9 kPa, and >9 kPa respectively.[18] For patients already on nucleoside analogue therapy, we additionally calculated the Fibrosis-4 Index (FIB-4 = age (yr) x AST [U/L]/(platelets [$10^9$/L] x (ALT [U/L])$^{1/2}$) at the time point of treatment commencement, with advanced fibrosis then defined as FIB-4 index >1.45.[18]

HBV DNA was quantified by the Cobas® HBV Test in a Cobas® 4800 System (Roche, Basel, Switzerland). The lower limit of quantification is 10 IU/mL, and the limit of detection is 4.4 IU/mL according to the manufacturer's protocol. Persistent HBV DNA undetectability was defined as at least three measurements over the past two years that were lower than the target detection limit (<4.4 IU/mL).

### Quantitative polymerase chain reaction (QPCR)

QPCR was performed to assess the relative abundance of the identified microbial genes involved in L-tryptophan biosynthesis in human fecal DNA samples using DNA Engine Opticon® 2 System for Real-Time PCR Detection (Bio-Rad Laboratories Inc, CA, USA) with SYBR Green I (Takara Bio Inc, Shiga, Japan) and specific primers. The used primers for TrpA and TrpB in this study were: TrpA forward 5′-TCTGTTTGCCCAG TTGAAGG-3′, TrpA reverse 5′-GGGATACCTAACTCC AGCG-3′; TrpB forward 5′-GGCAGGCGTTGCTGGC-GAAG-3′, TrpB reverse 5′-GTTAGGCGACTGGCGTT-CAA-3′.

### Supernatant exposure assay

An *Escherichia coli* strain (isolated from stool samples) growing overnight in fresh Brain Heart Infusion (BHI) broth (#53286, Sigma–Aldrich, St. Louis, MO, USA) was then sub-cultured 1:50 and grown for 24 h. Bacterial cultures were spun down at 11,000 g for 2 min and the supernatant was carefully removed without disturbing the pellet and through a 0.22-μM syringe filter to remove any remaining bacteria in the suspension. A human hepatic stellate cell (HSC)-LX-2 cell line (RRID: CVCL_5792) was cultured with 1:3 (25%) or 1:1 dilution (50%) supernatant of spent media from *Escherichia coli* or with L-tryptophan (0, 10, 50, 100, 200, 400 μM) for 24 h. Western blot was used to evaluate the expression of α-smooth muscle actin (α-SMA) and alpha-1 type I collagen (COL1A1) using α-SMA XP Rb mAb (RRID: AB_2734735) and COL1A1 XP Rb mAb (RRID: AB_2904565) after treatment.

### Full-length 16S sequencing for gut microbiota analysis

Fresh Stool DNA was extracted from the fecal samples using the Norgen Stool DNA Isolation Kit (#SKU27600, Norgen Biotek Corp, Thorol, Canada). Full-length 16S sequencing of stool DNA was performed using the PacBio Sequel system (PacBio Bio-Sciences, Menlo Park, CA, USA) at the Centre for PanorOmic Sciences Genomics Core, The University of Hong Kong. The complete process was performed according to the Full-Length 16S Amplification SMRTbell Template Preparation and Sequencing workflow as provided by PacBio.

### Circular consensus sequences (CCS) conversion

The conversion of raw sequencing data to CCS was performed through the SMRT Portal, the SMRTAnalysis software (v2.2.0) provided by PacBio Biosciences. Raw reads were demultiplexed by barcoding and subreads were assigned to individual samples. Five or greater full-pass subreads from the insert were used to generate a CCS read, which is highly accurate (~99% accuracy).

### Amplicon sequence variants generation and taxa inference

Demultiplexed CCS were subsequently analyzed using DADA2 algorithms.[19] Reads were first filtered by sequencing quality. An error model for the sequencing data was computed and used to infer unique amplicon sequence variants (ASV). An initial sequence table was constructed after chimaeras were identified and removed. Finally, taxonomy was assigned using DADA2 naïve RDP Bayesian classifier against the Silva 138 database with species annotation.[20] The ASVs with the taxonomy table generated were then used in downstream analysis.

For microbial gene prediction, the bacterial species for each enzyme from metabolic pathways was collected by searching the protein name or gene name in the UniProt database (https://www.uniprot.org/), and matched entries with bacterial species information.

### Clustering by partitioning around medoids (PAM) algorithm

To illustrate the compositional differences in the microbial populations, all samples were clustered using the PAM clustering algorithm as previously described.[21,22] The optimal number of clusters was determined when two indices, the Calinski-Harabasz (CH) index and average Silhouette width, were maximized.[23] CH index generally reflected the difference of the distances between/within clusters. The higher the CH index, the better the data points were partitioned into.[24,25] A positive Silhouette width of an individual sample indicated its similarity to its cluster concerning other clusters. Fecal microbiota samples were then clustered accordingly using the distance matrix calculated by the weighted UniFrac method at the genus level, which accounts for both the abundance and phylogenetics distance of genera shared between samples.

### Canonical correspondence analysis (CCA)

CCA was used to study the relationship between variables and gut microbiota community structures. CCA is a constrained ordination technique whose first axis is a linear combination of environmental variables that best explains variation in a matrix of species abundances. Additional orthogonal axes explain the remaining variance in the community data.[26] The lengths and positions of the arrows provide information about the relationship between the original environmental variables and the derived axes. Arrows that are parallel to an axis indicate a correlation; the length of the arrow indicates the strength of that correlation.

### Plasma bile acid quantification by LC-MS/MS

The quantification of plasma bile acids was performed by liquid chromatography-tandem mass spectrometry (LC-MS/MS) analysis at the Centre for PanorOmic Sciences Proteomics and Metabolomics Core, The University of Hong Kong. The chromatographic separation was carried out on an Acquity I-Class ultra-high-performance liquid chromatographic system by (Waters Corp Milford, MA, USA) using an ethylene bridged hybrid C18 column (2 mm × 100 mm). The mass spectrometry analysis was processed using a QTRAP®6500+ from Sciex Corp (Framingham, MA, USA). Data analysis was performed using the SciEX OS-Q Analysis Software (Framingham, MA, USA). Linear calibration curves for each analyte were generated by plotting peak area ratio of external/internal standard against authentic standard concentration at different concentration levels. Analytes were confirmed by comparing the retention time and ratio of characteristic transitions between the sample and standard.

### Statistical analysis

Numerical data were presented as median with interquartile range (IQR). Categorical variables were presented in n (%), and differences were assessed by Fisher's exact tests. Comparisons of continuous variables between two groups and more than two groups were made using Mann–Whitney U test and Kruskal–Wallis tests followed by Dunn's tests paired with Benjamini-Hochberg false rate discovery, respectively. All statistical analyses of the gut microbiome were performed with the R vegan package of R v4.2.2 software unless otherwise stated. All bacterial genera with a larger than 50% prevalence rate in either cluster were selected for correlation analysis. The valid association was filtered by $|rho|>0.3$ and $p < 0.05$ based on Spearman's rank correlation coefficient after Benjamini-Hochberg correction for multiple testing (unless otherwise specified). Univariate analyses were used to quantify associations between covariates and gut bacterial clusters, as well as between covariates and HBV DNA detectability. Multiple logistic regression models were used to quantify the associations between outcome measurements and microbiota features. The linear discriminant analysis (LDA) effect size (LEfSe)[27] was used to determine taxonomic biomarkers and the results were plotted with a log score cut-off of 3 (unless otherwise specified) to identify differentially abundant microbes in each taxon level between comparison groups.

### Ethics

Written informed consent was obtained for all patients. This study was approved by the Institutional Review Board, The University of Hong Kong and The Hong Kong West Cluster of the Hospital Authority, Hong Kong (Ref No: UW 19-751). All data were deidentified in the study. All investigations carried out in this study were performed following the Declaration of Helsinki and ICH GCP guidelines, local regulations, Hospital Authority, and university policies.

### Role of funders

The funders had no role in the study design, data collection and analysis, decision to publish, or preparation of the manuscript.

## Results

### The HBV cohort exhibited the presence of three distinct gut microbial clusters in CHB patients

The clinical characteristics of the 110 CHB patients are shown in Table S1. Their median age was 61.2 (IQR 57.3–65.7) years, and 72.7% of them were male (Table S1). All patients were HBeAg-negative. Sixty-one (55.5%) patients had steatosis, and fifty-two (47.3%) patients had F3/4 advanced liver fibrosis. Eighty-four of them were on nucleos(t)ide analogues treatment for a median duration of 98.1 (IQR 48.3–130.0) months. Fifty (45.5%) patients had undetectable plasma HBV DNA (<4.4 IU/mL).

Based on the PAM clustering algorithm, all fecal samples (n = 110) of our HBV cohort were optimally divided into three distinct microbial clusters, which were distinctly localized separately in a PCoA plot (Fig. 1a). PAM-cluster 1 (C1, n = 49), consisting of 44.5% gut bacterial communities, was separated from the second most common PAM-cluster 2 (C2, n = 44; 40.0%) along the PCoA axis 1; while PAM-cluster 3 (C3), including 17 (15.5%) data points, distinguished from the others along the PCoA axis 2. The dominant bacterial taxa (Fig. 1b) based on LefSe for C1, C2, and C3 were *Bacteroides* (log LDA score 5.33, $p < 0.01$, compared with the remaining taxa), *Blautia* (log LDA score 3.92, $p < 0.01$) and *Prevotella* (log LDA score 5.39, $p < 0.01$) respectively. The relative abundance of the above-mentioned bacterial taxa among different clusters is depicted in Fig. 1c. The three clusters were then characterized by their specific dominant genera and were labeled accordingly as c-*Bacteroides* (C1), c-*Blautia* (C2), and c-*Prevotella* (C3).

When comparing the microbial composition of the three clusters, c-*Bacteroides* was the least diverse, with decreased indices of alpha diversity (Shannon's Index: $p < 0.05$, Fig. 1d; and Chao1 richness: $p < 0.01$, Fig. 1e). c-*Blautia* was the most diverse cluster. Co-occurrence analysis demonstrated negative interactions between these three clusters (Fig. 1f): *Bacteroides* correlated negatively with the dominant bacterial taxa of c-*Blautia*; *Blautia* was found to co-occur positively with the bacterial genera being inhibited in the c-*Bacteroides*; *Prevotella* 9 demonstrated a negative interaction with *Bacteroides*.

### Bacterial signatures in c-*Bacteroides* attributed to unique bile acid profiles and different bile acid biotransformation pathways

Patients with gut microbial cluster c-*Bacteroides* had a higher plasma UDCAs level (including free UDCA, its derivatives GUDCA and TUDCA) than patients with c-*Blautia* (all $p < 0.05$, Table S2), and patients with gut microbial cluster c-*Bacteroides* had a significantly higher relative abundance of UDCAs than those with clusters c-*Blautia* and c-*Prevotella* (all $p < 0.05$, Fig. 2a).

The first two axes of canonical correspondence analysis explained 8.9% (CCA1: 5.1% and CCA2: 3.8%) of all variances (Fig. 2b). UDCA was nearly parallel to the CCA1 axis, indicating a strong positive association. The arrows for UDCA and GUDCA also followed a similar direction to how the c-*Bacteroides* clustered, consistent with the association between c-*Bacteroides* and UDCAs (Fig. 2a). The microbial genera including primarily those found enriched in c-*Bacteroides* (Table S3), namely *Flavonifractor*, *Lachnoclostridium*, *Bacteroides*, *Ruminococcus gnavus*, and *Fusobacterium*, were the only bacteria genera positively associated with UDCA bile acids (all $|rho|>0.3$ and $p < 0.05$, Fig. 2c). These five bacterial genera, corresponded to UDCA and GUDCA, which also correlated positively to CCA1 and CCA2 (Fig. 2d).

The proportion of bacteria that possessed 7-alpha-hydroxysteroid dehydrogenase (7α-HSDH), the protein for the first reaction in the synthesis of UDCA,[28] was significantly enriched in c-*Bacteroides* when compared to either c-*Blautia* or c-*Prevotella* (27.20% vs. 9.60% and 3.17% respectively, both $p < 0.001$, Fig. 3). The difference in the abundance of the second protein in UDCA biosynthesis, 7-beta-hydroxysteroid dehydrogenase (7β-HSDH), between c-*Bacteroides* and the other two clusters was insignificant ($p > 0.05$, Fig. 3). Accordingly, the abundances of the bacterial species that account for the proteins for LCA and DCA biotransformation (baiB, baiA, baiE, or baiF) were significantly lower in c-*Bacteroides* than in c-*Blautia* (baiB, 0.06% vs. 0.38%, $p < 0.01$; baiE, 0.20% vs. 1.03%, $p < 0.01$ baiF, 0.26% vs. 0.65%, $p = 0.002$, Fig. 3).

### Association of gut microbial clusters with plasma HBV DNA undetectability in nucleos(t)ide analogues-treated patients

When comparing the three microbial clusters in on-treatment patients, there were significant differences in fibrosis staging, proportion of patients with undetectable plasma HBV DNA, ALT, and albumin (all $p < 0.05$, Table 1). Microbial cluster c-*Bacteroides* was significantly associated with higher odds of undetectable HBV DNA (<4.4 IU/mL) (odds ratio: OR 3.49, 95% confident interval: 95% CI 1.43–8.96, $p = 0.01$, Table 2) when compared with non-c-*Bacteroides* clusters. On the other hand, c-*Blautia* was inversely associated with glycated hemoglobin (OR 0.66, 95% CI 0.43–0.98, $p = 0.05$) while positively associated with fibrosis (OR 2.74, 95% CI 1.09–7.31, $p = 0.04$, Table 2). c-*Prevotella* was negatively associated with albumin (OR 0.78, 95% CI 0.65–0.91, $p < 0.01$) and ALT level (OR 0.94, 95% CI 0.89–0.99, $p = 0.02$, Table 2). No significant differences and associations were found in treatment-naïve patients (Table 2 and Table S4). Similar associations were also observed using a multinomial logistic regression analysis for these three gut microbial clusters (Table S5).

Canonical correspondence analysis showed that the first two axes explained 6.3% (CCA1: 3.6% and CCA2: 2.7%) of all variances (Fig. 4a and b). Consistent with the results from logistic regression, undetectable HBV DNA colocalized and associated positively with c-*Bacteroides* bacterial communities (Fig. 4a), including *Bacteroides*, *Lachnoclostridium*, and *Flavonifractor*, together with *Bilophila*, *Parabacteroides*, *Phascolarctobacterium*, and *Ruminococcus gnavus* (Fig. 4b). All above bacteria associated with undetectable HBV DNA were all found enriched in the gut microbial cluster c-*Bacteroides* as shown in the LEfSe analysis (Table S3), further validating the relationship between c-*Bacteroides* and undetectable HBV-DNA. Moreover, c-*Bacteroides* remained significantly associated with undetectable HBV-DNA

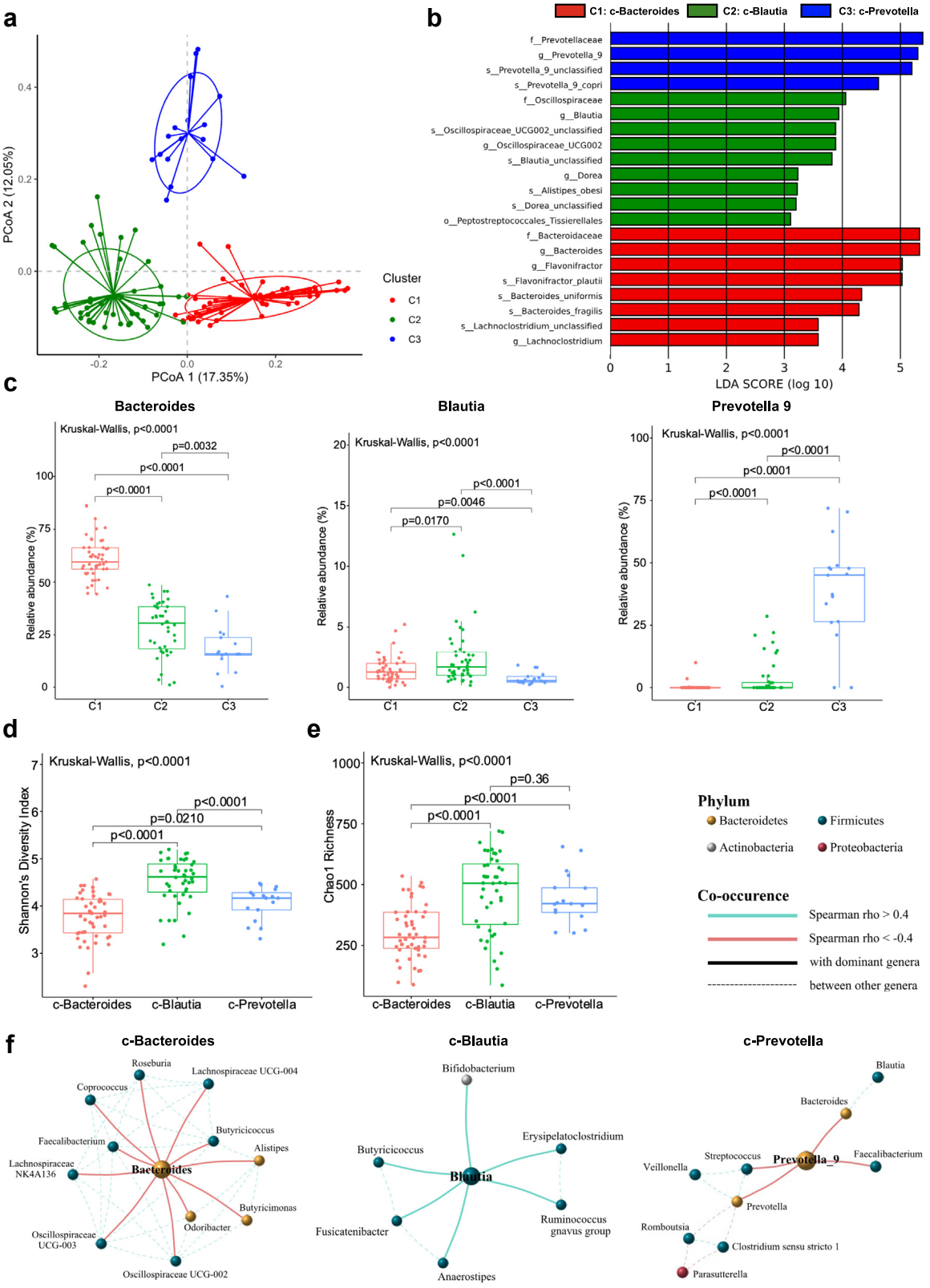
a
PCoA 2 (12.05%)
PCoA 1 (17.35%)
Cluster
C1
C2
C3
b
C1: c-Bacteroides
C2: c-Blautia
C3: c-Prevotella
f__Prevotellaceae
g__Prevotella_9
s__Prevotella_9_unclassified
s__Prevotella_9_copri
f__Oscillospiraceae
g__Blautia
s__Oscillospiraceae_UCG002_unclassified
g__Oscillospiraceae_UCG002
s__Blautia_unclassified
g__Dorea
s__Alistipes_obesi
s__Dorea_unclassified
o__Peptostreptococcales_Tissierellales
f__Bacteroidaceae
g__Bacteroides
g__Flavonifractor
s__Flavonifractor_plautii
s__Bacteroides_uniformis
s__Bacteroides_fragilis
s__Lachnoclostridium_unclassified
g__Lachnoclostridium
LDA SCORE (log 10)
c
Bacteroides
Blautia
Prevotella 9
Kruskal-Wallis, p<0.0001
Relative abundance (%)
C1
C2
C3
d
Shannon's Diversity Index
e
Chao1 Richness
c-Bacteroides
c-Blautia
c-Prevotella
Phylum
Bacteroidetes
Firmicutes
Actinobacteria
Proteobacteria
Co-occurence
Spearman rho > 0.4
Spearman rho < -0.4
with dominant genera
between other genera
f
c-Bacteroides
Roseburia
Lachnospiraceae UCG-004
Coprococcus
Butyricicoccus
Faecalibacterium
Alistipes
Lachnospiraceae NK4A136
Bacteroides
Butyricimonas
Odoribacter
Oscillospiraceae UCG-003
Oscillospiraceae UCG-002
c-Blautia
Bifidobacterium
Erysipelatoclostridium
Butyricicoccus
Blautia
Ruminococcus gnavus group
Fusicatenibacter
Anaerostipes
c-Prevotella
Blautia
Bacteroides
Streptococcus
Prevotella_9
Faecalibacterium
Veillonella
Prevotella
Romboutsia
Clostridium sensu stricto 1
Parasutterella

after adjusting for the covariates associated with gut microbial clusters (adjusted OR 5.66, 95% CI 2.06–17.28, p = 0.001, Table S6).

### The potential role of gut microbiome in HBV-related advanced fibrosis after successful virological control

Our previous regression analysis showed that microbial cluster c-*Blautia* was significantly associated with higher odds of advanced fibrosis (Table 2) in on-treatment patients. 54.8% (n = 46) of on-treatment HBV patients were under successful virological control (defined as having undetectable HBV DNA <4.4 IU/mL). The differences in clinical characteristics of patients with or without advanced fibrosis are depicted in Table 3. The total bile acids, conjugated bile acids, primary bile acids, and primary conjugated bile acids were significantly higher in patients with advanced fibrosis when compared with those without advanced fibrosis in patients with undetectable HBV-DNA, manifested as a significant increase in plasma levels of cholic acid (CA), glycocholic acid (GCA), chenodeoxycholic acid (CDCA), glycochenodeoxycholic acid (GCDCA), taurochenodeoxycholic acid (TCDCA), and glycoursodeoxycholic acid (GUDCA) as well as tauroursodeoxycholic acid (TUDCA) (all p < 0.05, Table S7). In patients with detectable HBV-DNA, no significant differences in plasma primary bile acids and primary conjugated bile acids were observed between patients with and without advanced fibrosis in patients with detectable HBV-DNA (Table S7).

In the undetectable HBV-DNA group, biomarker discovery analysis-Lefse showed that *Escherichia coli* was significantly enriched in those with advanced fibrosis, the highest LDA score of which was 9.20 (p = 0.0337), while *Alistipes shahii* was significantly enriched in those without advanced fibrosis with the highest LDA score 8.18 (p = 0.0120) at the species level when comparing between patients with and without advanced fibrosis (Fig. 5a). Patients with advanced fibrosis had a lower relative abundance of *Alistipes shahii* (0.04% vs. 0.32%, p = 0.015, Fig. 5b) and a higher relative abundance of *Escherichia coli* (0.21% vs. 0.03%, p = 0.035, Fig. 5c). Besides, *Alistipes obesi*, *Blautia stercoris*, *Desulfovibrio piger*, *Roseburia hominis*, and *Ruminococcus callidus* were significantly decreased in HBV patients with advanced fibrosis when compared to those without advanced fibrosis (all p < 0.05, Fig. 5b). No significant differences were observed in alpha-diversity indices (Shannon's diversity index and Chao1 richness) between HBV patients with or without advanced fibrosis (all p > 0.05, Fig. 5d and e). These downregulated bacterial signatures in advanced fibrosis were correlated negatively with the altered BAs, fasting blood glucose, and liver stiffness values while upregulated bacterial signature-*Escherichia coli* was positively correlated with liver stiffness, fasting blood glucose, GGT, CDCA, UDCA and GUDCA (all |rho|>0.3, p < 0.05, Fig. 5f). Our microbial function analysis showed that superpathway of L-tryptophan biosynthesis significantly enriched in patients with advanced fibrosis (LDA score 2.67, p = 0.0008, Fig. 5g) while L-arginine biosynthesis pathways were enriched in patients without advanced fibrosis. Moreover, L-tryptophan biosynthesis was correlated positively with *Escherichia coli*, liver stiffness, and fasting blood glucose while L-arginine biosynthesis pathways were correlated positively with *Blautia stercoris* and *Roseburia hominis* (all |rho|>0.3, p < 0.05, Fig. 5h). The QPCR results showed a significant increase in the expression of TryA and TryB genes, which encode key enzymes involved in L-tryptophan biosynthesis, in patients with advanced fibrosis when compared to those without advanced fibrosis (p = 0.025 and 0.011, respectively, Figure S2).

## Discussion

In this study, based on gut microbial compositions, we identified three clusters among the CHB patients, which were dominated by the genera *Bacteroides*, *Blautia*, and *Prevotella* respectively. We found that CHB patients with different gut microbial clusters had distinct clinical characteristics. Specifically and interestingly, gut microbial cluster c-*Bacteroides* was associated with undetectable HBV-DNA (plasma HBV DNA <4.4 IU/mL) in patients with antiviral therapy. To our knowledge, this is the first study that demonstrates a linkage between c-*Bacteroides* and HBV treatment response during nucleos(t)ide analogues therapy (Fig. 6).

Patients with gut microbial cluster c-*Bacteroides* were enriched with UDCAs. The five bacterial genera found enriched in c-*Bacteroides*, namely *Flavonifractor*,

***Fig. 1:*** **The HBV cohort exhibited the presence of three distinct gut microbial clusters. (a)** The distribution of gut bacterial communities in the Principal Co-ordinates Analysis (PCoA) plot in different clusters at the genus level. **(b)** Differential gut bacterial taxa between three clusters were determined by Linear discriminant analysis Effect Size analysis (LEfSe) and the results were plotted with a threshold of log LDA score greater than 3 and false discovery rate (FDR) smaller than 0.05. **(c)** Relative abundances of the dominant genus in these three clusters. Post hoc pairwise comparison between multiple groups was assessed by the Dunn's test with Benjamini-Hochberg correction after the Kruskal–Wallis test. **(d)** Shannon's index and **(e)** Chao 1 richness of three microbial clusters. **(f)** Co-occurrence analysis between the dominant taxon of each gut microbial signature and other bacterial genus was performed by Spearman's correlation. The prevalence of bacterial genera greater than 30% in the cluster was filtered for subsequent all to all correlation analysis. Valid interactions, defined as the absolute value of Spearman's |rho|>0.4 and p < 0.05, were plotted in the correlation network. Green line, positive correlation; red line, negative correlation; solid line, correlation with the dominant taxon of the cluster; dotted line, correlation among other bacterial taxa.

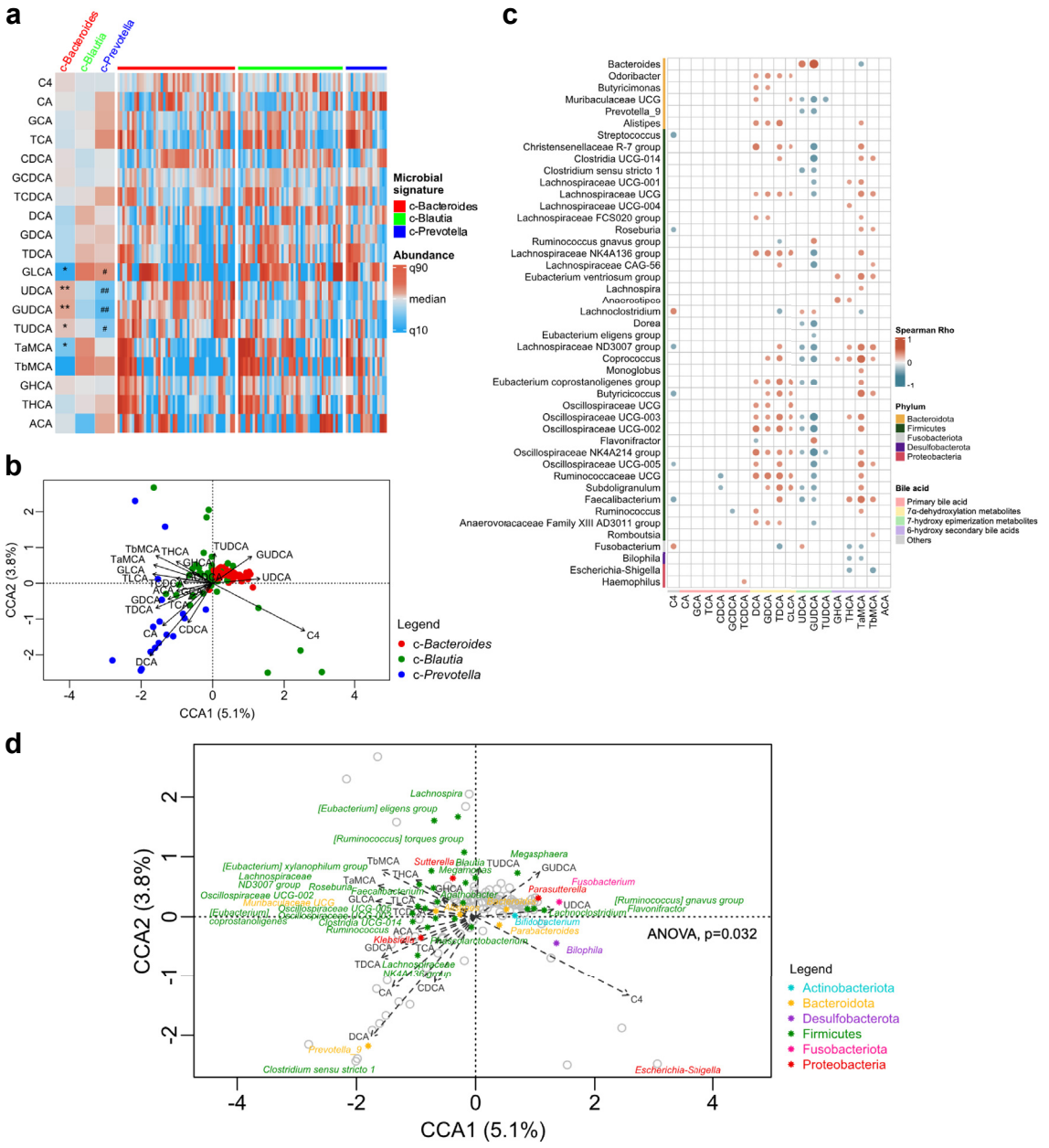


*Fig. 2:* **Distinct bile acid signatures in c-Bacteroides were linked to differential abundance in bacteria species. (a)** Heatmap of individual BA species in each individual and in each microbial cluster. **(b)** Canonical correspondence analysis (CCA) analysis between bile acids and individual gut microbial communities. The community data points were colored according to their microbial clusters. **(c)** Correlation heatmap between bacterial genus and bile acid. All bacterial genera with a larger than 50% prevalence rate in either cluster were selected for correlation analysis. The valid association was filtered by |rho|>0.3 and $p < 0.05$ after Benjamini–Hochberg correction for multiple testing. **(d)** CCA analysis between bile acids and bacterial genera. Only the 30 most abundant genera were displayed. The first 2 CCA dimensions were shown, and the percentage of the total variance each dimension explained was indicated. The lengths and positions of the arrows provide information about the relationship between the original environmental variables and the derived axes. Arrows that are parallel to an axis indicate a correlation; the length of the arrow indicates the strength of that correlation. Significance was computed by 999 permutations.

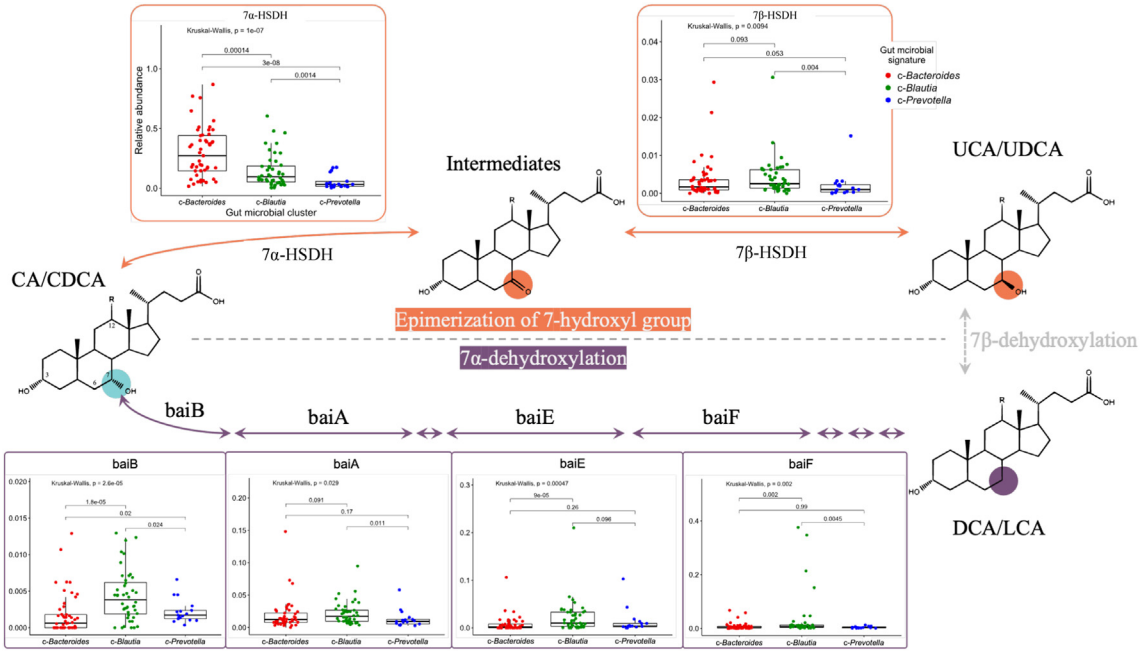


***Fig. 3:*** **The altered bile acid profiles were corresponding to different secondary BA biotransformation pathways by gut microbiota**. Relative abundance of microbial gene 7α-HDSH, 7β-HDSH, baiB, baiA, baiE, and baiF. Two bile acid biotransformation pathways, namely 7α-dehydroxylation and 7-hydroxy epimerization, were selectively extracted from the metabolic pathway of secondary bile acid biotransformation in UniProt database. Post hoc pairwise comparison between multiple groups was assessed by Dunn's test with Benjamini-Hochberg false discovery rate (FDR) correction after the Kruskal–Wallis test. *p_{FDR} <0.05.

*Lachnoclostridium*, *Bacteroides*, *Ruminococcus gnavus*, and *Fusobacterium*, were the only bacteria genera positively associated with UDCA bile acids. The proportion of bacteria possessed with 7α-HSDH, the protein for the first reaction in the synthesis of UDCA, was significantly enriched in c-*Bacteroides* when compared to either c-*Blautia* or c-*Prevotella* (Fig. 3). One critical step for the viral entry involves the specific interaction between the large Hepatitis B surface antigen (HBsAg) protein of the virus and the receptor NTCP of the host.[29] The beneficial effect of UDCAs as substrates of NTCP was demonstrated in in-vitro experiments. UDCAs inhibited HBV infection in HBV susceptible cell line models at the IC-50 of about 20–100 μM.[15,30,31] Consistently, in our study, CHB patients with gut microbial cluster c-*Bacteroides*, had a higher circulating level of UDCAs than HBV patients with other gut microbial clusters, and was associated with virological undetectability during nucleos(t)ide analogue therapy. Despite that distinct bile acid profiles were identified among the three groups, the differences in the level of C4, the intermediate of bile acid synthesis, were minimal and not statistically significant, suggesting that the gut microbiota-associated alteration in bile acid profile was related to secondary BA biotransformation rather than hepatic bile acid synthesis.

It has reported the bacterial signature for entecavir treatment signature, demonstrating that, when compared to treatment-naïve CHB patients, certain bacterial groups such as *Blautia*, *E. hallii* group, and *Ruminococcaceae_UCG-013* were enriched in patients receiving entecavir treatment.[32] In our cohort, specific microbial differences between treatment-naïve and on-treatment patients were also observed (Figure S1). Notably, the bacterial genera enriched in the c-*Bacteroides* cluster were associated with undetectable HBV-DNA in patients receiving nucleos(t)ide analogues therapy (Fig. 4). One possible reason for the association between gut microbiome and treatment response may lie in the probiotic properties of gut microbiota and their ability to modulate host immunity.[33–35] In one study, *Flavonifractor plautii*, a bacterial taxon enriched in c-*Bacteroides*, was found to increase mRNA expression of IFN-γ and IL-10 in splenocytes.[36] These bacteria, enriched in c-*Bacteroides* and correlated with undetectable HBV-DNA in the present study, are likely to be capable of modulating host immunity. Therefore, CHB patients with the c-*Bacteroides* signature may exhibit a different immune status compared to those with other gut microbial clusters, potentially affecting their response to nucleos(t)ide analogues therapy. This could be attributed to the achievement of an undetectable viral

| | *c-Bacteroides* (n = 38) | *c-Blautia* (n = 31) | *c-Prevotella* (n = 15) | p_{FDR} |
|---|---|---|---|---|
| **Gender** | | | | 0.652 |
| Male | 28 (73.7%) | 25 (80.6%) | 11 (73.3%) | |
| Female | 10 (26.3%) | 6 (19.4%) | 4 (26.7%) | |
| Age (years) | 60.4 (57.1–66.6) | 64.6 (61.1–68.3) | 60.7 (54.4–65.7) | 0.235 |
| **Steatosis** | | | | 0.330 |
| Non-Steatosis | 13 (34.2%) | 15 (48.4%) | 8 (53.3%) | |
| Steatosis | 25 (65.8%) | 16 (51.6%) | 7 (46.7%) | |
| **Fibrosis** | | | | 0.033 |
| No advanced liver fibrosis (<F3) | 20 (52.6%) | 9 (29.0%) | 10 (66.7%) | |
| Advanced liver fibrosis (F3/4) | 18 (47.4%) | 22 (70.1%) | 5 (33.3%) | |
| **Plasma HBV DNA** | | | | 0.024 |
| Undetectable | 27 (71.1%) | 13 (41.9%) | 6 (40.0%) | |
| Detectable | 11 (28.9%) | 18 (58.1%) | 9 (60.0%) | |
| BMI (kg/m$^2$) | 25.0 (22.7–28.4) | 25.8 (23.0–28.1) | 27.0 (24.3–29.6) | 0.349 |
| CAP (dB/m) | 291.0 (239.5–318.5) | 281.0 (227.0–305.0) | 242.0 (227.0–340.0) | 0.572 |
| Liver Stiffness (kPa) | 9.0 (5.2–14.3) | 10.3 (5.7–13.8) | 5.7 (5.2–12.8) | 0.334 |
| Fasting blood glucose (mmol/L) | 6.5 (5.3–7.6) | 6.3 (5.4–7.7) | 6.2 (4.9–9.1) | 0.980 |
| HbA1c (%) | 6.7 (5.6–7.2) | 5.6 (5.3–6.8) | 6.0 (5.2–7.7) | 0.140 |
| Triglyceride (mmol/L) | 1.2 (0.8–1.9) | 1.2 (0.8–1.5) | 1.1 (0.8–1.2) | 0.447 |
| Total cholesterol (mmol/L) | 4.2 (3.8–5.1) | 4.3 (3.6–5.2) | 3.7 (3.5–4.8) | 0.538 |
| HDL-cholesterol (mmol/L) | 1.3 (1.1–1.4) | 1.3 (1.0–1.5) | 1.3 (1.0–1.8) | 0.996 |
| LDL-cholesterol (mmol/L) | 2.3 (1.8–3.2) | 2.5 (1.6–3.3) | 2.2 (1.8–2.8) | 0.807 |
| ALT (U/L) | 36.0 (23.5–54.5) | 29.0 (23.0–52.0) | 28.0 (18.0–30.0) # | 0.040 |
| AST (U/L) | 35.0 (25.0–40.5) | 33.0 (25.0–38.0) | 24.0 (23.0–32.0) | 0.086 |
| GGT (U/L) | 39.0 (24.0–76.0) | 39.0 (26.0–72.0) | 25.0 (19.0–43.0) | 0.165 |
| ALP (U/L) | 67.0 (59.0–79.0) | 65.0 (55.0–76.0) | 72.0 (65.0–79.0) | 0.343 |
| Albumin (g/L) | 47.0 (44.6–49.0) | 46.0 (44.0–49.0) | 44.0 (40–46.0) # | 0.010 |
| Total Bilirubin (μmol/L) | 12.0 (10.0–17.0) | 13.0 (10.0–17.0) | 10.0 (8.0–15.0) | 0.634 |
| Platelet (x 10$^9$/L) | 194.0 (155.0–247.0) | 170.0 (125.0–224.0) | 167.0 (122.0–237.0) | 0.158 |
| **Antiviral treatment** | | | | 0.433 |
| ETV | 26 | 26 | 13 | |
| TDF/TAF | 11 | 5 | 2 | |
| Telbivudine | 1 | 0 | 0 | |
| **Treatment duration (months)** | 102.2 (48.2–127.9) | 96.0 (23.2–129.1) | 97.7 (52.4–134.3) | >0.999 |

Non-steatosis was defined as CAP <248 dB/m, steatosis was defined as CAP ≥248 dB/m. No advanced liver fibrosis (<F3), and advanced liver fibrosis (F3/4) were defined as liver stiffness ≤9 kPa, and >9 kPa respectively. Undetectable plasma HBV DNA was defined as <4.4 IU/mL. Numerical data were presented as median (interquartile range). Post hoc pairwise comparison between multiple groups was assessed by the Dunn's test with Benjamini-Hochberg false discovery rate (FDR) correction after the Kruskal–Wallis test. *p_{FDR} <0.05, **p_{FDR} <0.01 for *c-Bacteroides* vs. *c-Blautia*;^p_{FDR} <0.05,^p_{FDR} <0.01 for *c-Blautia* vs. *c-Prevotella*; #p_{FDR} <0.05, ##p_{FDR} <0.01 for *c-Bacteroides* vs. *c-Prevotella*. Categorical variables were presented in n (%), and differences were assessed by Fisher's exact tests. CAP, controlled attenuation parameter; LSM, liver stiffness measurement; BMI, body mass index; HbA1c, glycated hemoglobin; HDL, high-density lipoprotein; LDL, low-density lipoprotein; ALT, alanine transaminase; AST, aspartate aminotransferase; GGT, gamma-glutamyl transferase; ALP, alkaline phosphatase; ETV, entecavir; TDF, tenofovir disoproxil fumarate; TAF, tenofovir alafenamide.

***Table 1:*** **Clinical characteristics in on-treatment HBV patients with different gut microbial clusters.**

load due to an enhanced adaptive immune response triggered by gut bacteria.

While *Blautia* is an anaerobic genus known for its probiotic characteristics and its potential to alleviate metabolic syndrome, our study emphasized its effect on the progression of fibrosis in CHB patients receiving antiviral therapy (Table 2 & Fig. 4). 54.8% of on-treatment CHB patients in this study achieved successful virological suppression with undetectable HBV-DNA after nucleos(t)ide analogues therapy. Gut microbial dysbiosis can persist and contribute to liver fibrosis progression even after virological control is achieved in patients with chronic hepatitis B. While one of the ultimate goals of viral suppression in CHB patients is to reduce the risk of development of fibrosis or other related complications, some patients may progress to liver fibrosis even after viral suppression is achieved. 26/46 (57%) of patients with undetectable HBV-DNA in this study developed advanced fibrosis (Table 3). Further investigations on the role of gut microbiome in HBV-related advanced fibrosis are needed to understand the mechanisms involved and predict the risk of fibrosis

| Factors | c-*Bacteroides* | | | c-*Blautia* | | | c-*Prevotella* | | |
|---|---|---|---|---|---|---|---|---|---|
| | Odds ratio (95% CI) | | p | Odds ratio (95% CI) | | p | Odds ratio (95% CI) | | p |
| **All** | | | | | | | | | |
| Albumin | 1.07 | (0.97–1.21) | 0.20 | 1.07 | (0.96–1.20) | 0.25 | 0.81 | (0.69–0.92) | 0.00* |
| ALT | 1.01 | (1.00–1.04) | 0.15 | 1.00 | (0.98–1.01) | 0.59 | 0.96 | (0.91–0.99) | 0.05* |
| Undetectable HBV-DNA | 2.36 | (1.10–5.17) | 0.03* | 0.46 | (0.20–1.00) | 0.05* | 0.81 | (0.27–2.30) | 0.70 |
| Advanced fibrosis | 0.78 | (0.33–1.86) | 0.58 | 2.74 | (1.09–7.31) | 0.04* | 0.32 | (0.09–1.01) | 0.06 |
| HemoglobinA1c | 1.41 | (1.02–2.00) | 0.04* | 0.62 | (0.42–0.89) | 0.01* | 1.13 | (0.73–1.71) | 0.56 |
| **On-Treatment** | | | | | | | | | |
| Albumin | 1.11 | (0.99–1.26) | 0.10 | 1.07 | (0.95–1.21) | 0.28 | 0.78 | (0.65–0.91) | 0.00* |
| ALT | 1.02 | (1.00–1.04) | 0.11 | 1.00 | (0.98–1.01) | 0.63 | 0.94 | (0.89–0.99) | 0.02* |
| Undetectable HBV-DNA | 3.49 | (1.43–8.96) | 0.01* | 0.44 | (0.17–1.07) | 0.07 | 0.48 | (0.15–1.49) | 0.21 |
| Advanced fibrosis | 0.78 | (0.33–1.86) | 0.58 | 2.74 | (1.09–7.31) | 0.04* | 0.32 | (0.09–1.01) | 0.06 |
| HemoglobinA1c | 1.32 | (0.93–1.93) | 0.13 | 0.66 | (0.43–0.98) | 0.05* | 1.12 | (0.71–1.74) | 0.61 |
| **Treatment-Naïve** | | | | | | | | | |
| Albumin | 0.84 | (0.57–1.19) | 0.34 | 1.06 | (0.75–1.53) | 0.73 | 1.80 | (0.80–8.09) | 0.28 |
| ALT | 0.98 | (0.92–1.05) | 0.60 | 1.01 | (0.95–1.08) | 0.74 | 1.02 | (0.89–1.12) | 0.73 |
| Undetectable HBV-DNA | 0.40 | (0.02–3.70) | 0.46 | 1.00 | (0.10–9.59) | 1.00 | 7.00 | (0.24–214) | 0.21 |
| Advanced fibrosis | 0.28 | (0.01–2.26) | 0.28 | 1.65 | (0.23–14.57) | 0.62 | 5.00 | (0.17–146) | 0.29 |
| HemoglobinA1c | 1.99 | (0.87–6.05) | 0.15 | 0.51 | (0.16–1.18) | 0.17 | 0.90 | (0.10–3.13) | 0.89 |

No advanced liver fibrosis (<F3), and advanced liver fibrosis (F3/4) were defined as liver stiffness ≤9 kPa, and >9 kPa respectively. Undetectable plasma HBV DNA was defined as <4.4 IU/mL. *p < 0.05.

***Table 2:*** **Association of clinical parameters with gut microbial clusters in all HBV patients by regression analysis.**

progression. This study also unveils the potential of modulation of gut microbiome to improve treatment outcomes in CHB patients.

There was a significant enrichment in *Escherichia coli* and a significant decrease in *Alistipes shahii*, *Alistipes obesi*, *Blautia stercoris*, *Desulfovibrio piger*, *Roseburia hominis*, and *Ruminococcus callidus* in CHB patients with advanced fibrosis when compared to those without advanced fibrosis after successful virological suppression (Fig. 5). Similar findings of *Escherichia coli* signatures being associated with advanced fibrosis have been reported for NAFLD.[37] With persistent HBV DNA undetectability, gut microbiome changes may reflect the non-viral elements contributing to liver fibrogenesis. Animal studies have shown that *Escherichia coli* exacerbates HFD-induced fibrosis in mice via its flagellin,[38] however, treatment with *Escherichia coli* alone does not induce liver fibrosis.[39] The underlying mechanism may involve the bacterial translocation of *Escherichia coli* facilitated by the disrupted gut barrier. Interestingly, the presence of specific microbiome alterations in patients with advanced liver fibrosis was further linked to distinct functional changes, specifically related to *Escherichia coli*-mediated L-tryptophan (Fig. 5h), which is consistent with previous reports.[40,41] Tryptophan supplementation in animal models has yielded controversial outcomes. These controversial outcomes may reflect the different conditions in which tryptophan is skewed to produce different metabolites-proinflammatory or anti-inflammatory.[42] Treatment with L-tryptophan in

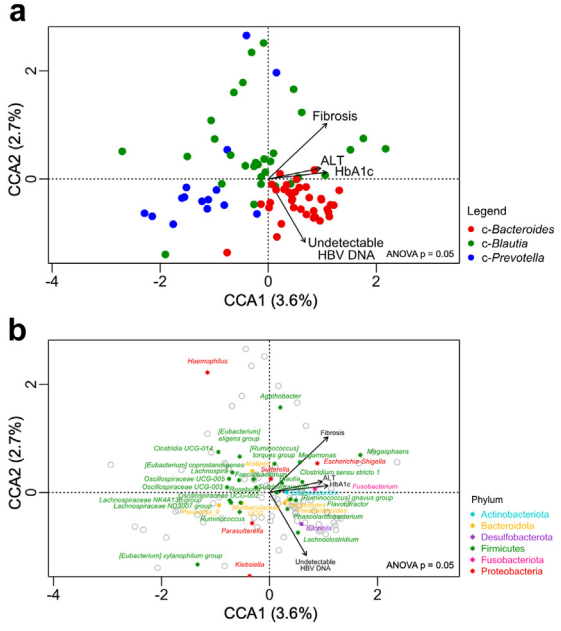


***Fig. 4:*** **The influential factors in three gut microbial clusters of nucleos(t)ide analogues (NAs)-treated HBV patients.** Canonical correspondence analysis (CCA) was used to study the relationship between variables and gut microbiota community structures. **(a)** CCA analysis between individual gut microbial communities (circles) and clinical parameters (arrows); **(b)** CCA analysis between clinical variables (arrows) and bacterial genera (star signs). Gut microbial communities (as grey circles) were also displayed. Only the 30 most abundant genera were shown in the plot.

| | Undetectable HBV DNA | | | Detectable HBV DNA | | |
|---|---|---|---|---|---|---|
| | No advanced liver fibrosis (n = 20) | Advanced liver fibrosis (n = 26) | p | No advanced liver fibrosis (n = 17) | Advanced liver fibrosis (n = 21) | p |
| Male, n (%) | 15 (75.0%) | 18 (69.2%) | 0.75 | 14 (82.4%) | 17 (81.0%) | 1.00 |
| Age (years) | 62.5 (59.0–66.2) | 64.4 (57.8–71.1) | 0.48 | 56.8 (47.8–61.3) | 65.0 (60.3–69.2) | 0.12 |
| BMI (kg/m$^2$) | 23.6 (22.5–27.0) | 25.5 (23.7–29.3) | 0.14 | 24.8 (22.8–27.8) | 26.6 (24.0–30.0) | <0.01 |
| CAP (dB/m) | 263.0 (221.5–314.3) | 288.0 (212.8–330.5) | 0.68 | 243.0 (227.0–314.0) | 296.0 (243.5–321.5) | 0.10 |
| Liver Stiffness (kPa) | 5.2 (4.0–5.8) | 12.4 (10.1–15.5) | <0.01 | 5.3 (4.7–5.7) | 12.4 (11.4–16.5) | <0.01 |
| Fasting blood glucose (mmol/L) | 5.6 (5.1–6.5) | 7.1 (5.8–7.7) | 0.01 | 5.9 (5.0–8.4) | 7.0 (5.6–8.7) | 0.21 |
| HbA1c (%) | 5.7 (5.2–6.5) | 6.6 (5.5–7.1) | 0.10 | 5.6 (5.4–7.2) | 6.8 (5.5–7.5) | 0.35 |
| Triglyceride (mmol/L) | 1.2 (0.8–1.4) | 1.1 (0.9–1.6) | 0.49 | 0.8 (0.7–1.4) | 1.2 (0.9–1.7) | 0.14 |
| Total cholesterol (mmol/L) | 4.7 (3.6–5.1) | 4.0 (3.7–5.2) | 0.75 | 4.2 (3.5–5.1) | 4.0 (3.6–5.2) | 0.91 |
| HDL-cholesterol (mmol/L) | 1.3 (1.0–1.8) | 1.3 (1.0–1.4) | 0.35 | 1.2 (1.1–1.6) | 1.2 (1.1–1.4) | 0.86 |
| LDL-cholesterol (mmol/L) | 2.7 (1.8–3.3) | 2.1 (1.8–3.1) | 0.74 | 2.3 (1.7–3.1) | 2.3 (1.7–3.2) | 0.91 |
| ALP (U/L) | 67.0 (57.5–71.8) | 68.0 (57.8–80.8) | 0.60 | 74.0 (62.0–89.0) | 65.0 (57.0–79.5) | 0.35 |
| ALT (U/L) | 24.0 (20.0–35.3) | 36.5 (23.8–53.0) | 0.22 | 33.0 (26.0–43.0) | 30.0 (23.5–55.5) | 0.66 |
| AST (U/L) | 26.5 (23.3–36.0) | 35.5 (25.8–40.3) | 0.03 | 25.0 (21.0–37.0) | 34.0 (28.0–49.0) | 0.06 |
| GGT (U/L) | 25.5 (16.0–35.0) | 42.5 (29.0–75.5) | <0.01 | 25.0 (19.5–41.5) | 68.0 (38.0–97.0) | <0.01 |
| Platelet ( × 10$^9$/L) | 184.0 (146.3–285.5) | 181.0 (86.0–233.8) | 0.27 | 208.0 (166.0–246.0) | 167.0 (121.0–226.0) | 0.09 |
| Albumin (g/L) | 46.5 (44.0–49.5) | 47.0 (42.8–49.0) | 0.86 | 46.0 (44.0–47.0) | 45.0 (44.5–48.5) | 0.50 |
| Total Bilirubin (umol/L) | 12.0 (7.0–17.0) | 13.5 (11.0–20.5) | 0.07 | 10.0 (8.0–13.0) | 12.0 (8.5–14.0) | 0.56 |
| Initial fibrosis status prior to antiviral treatment | | | | | | |
| FIB-4 | 1.85 (1.10–2.43) | 2.41 (1.48–3.92) | 0.03 | 1.48 (0.96–2.09) | 2.35 (1.41–4.04) | 0.04 |

Undetectable HBV DNA defined as <4.4 IU/mL Detectable HBV DNA included patients with detectable but nonquantifiable viral load, within the range of 4.4–10 IU/mL. Initial fibrosis status prior to antiviral treatment was determined by the Fibrosis-4 (FIB-4) index. BMI, body mass index; CAP, controlled attenuation parameter; FIB-4, fibrosis-4; HbA1c, glycated hemoglobin; HDL, high-density lipoprotein; LDL, low-density lipoprotein; ALP, alkaline phosphatase; ALT, alanine transaminase; AST, aspartate aminotransferase; GGT, gamma-glutamyl transferase.

***Table 3:*** **Comparison of clinical characteristics in on-treatment patients with and without advanced liver fibrosis under different HBV-DNA subgroups.**

combination with a high-fat, high-fructose diet exacerbated hepatic steatosis and fibrosis through serotonin-mediated activation of mTOR.[40,43] However, L-tryptophan alone did not induce these effects. Thus, there is no direct association between *Escherichia coli*-related metabolites and liver fibrosis (Figure S3). Other dysregulated microbes and metabolites may also contribute to the process of liver fibrosis, highlighting the importance of considering multiple microbial interactions in disease progression.

In NAs-treated CHB patients, we observed significantly higher levels of plasma primary bile acids (CA, GCA, CDCA, GCDCA, and TCDCA) in patients with advanced fibrosis compared to those without advanced fibrosis, particularly in patients with undetectable HBV-DNA. Interestingly, these significant differences were not observed between patients with and without advanced fibrosis in those with detectable HBV-DNA (Table S7). Our correlation analysis revealed that downregulated bacterial signatures (e.g., *Alistipes shahii*) in advanced fibrosis were negatively correlated with liver stiffness, fasting blood glucose, and altered BAs (Fig. 5f). In line with our findings, previous studies have demonstrated that primary bile acids such as GCA and GCDCA exhibit robust positive correlations with FibroScan LSM.[44] Interestingly, *Alistipes shahii* displayed a negative correlation with total primary bile acids and GCDCA.[44] Existing evidence suggests that liver fibrosis may be linked to the activation of the inflammasome pathway by CDCA[45] or GCDCA.[46] A relevant study[47] demonstrated that a combination of different serum metabolites, including GCA, could serve as a non-invasive blood-based diagnostic test for advanced fibrosis in NAFLD participants. Despite the intriguing correlation between diminished bacterial signatures and bile acid metabolism, the current lack of comprehensive experimental evidence hampers our understanding of their role in advanced fibrosis after successful virological control. Future *in-vivo* animal studies utilizing a murine model with induced liver fibrosis should explore whether interventions such as fecal microbiota transplantation from patients without advanced fibrosis or administration of single or multiple strains (e.g., *Alistipes shahii*, *Alistipes obesi*, *Ruminococcus callidus*) can contribute to fibrosis regression by reducing primary bile acids such as CDCA and GCDCA.

*Alistipes* dysbiosis can be either beneficial or harmful, but studies consistently suggest that a reduction in *Alistipes shahii* is linked to liver disease progression[48] and is more commonly found in both compensated and decompensated liver cirrhosis patients when compared to healthy controls.[49] Additionally, administering probiotics has been shown to increase the abundance of *Alistipes shahii* in mice, potentially leading to anti-inflammatory effects in HCC.[50] Notably, *Alistipes shahii*, which was enriched in

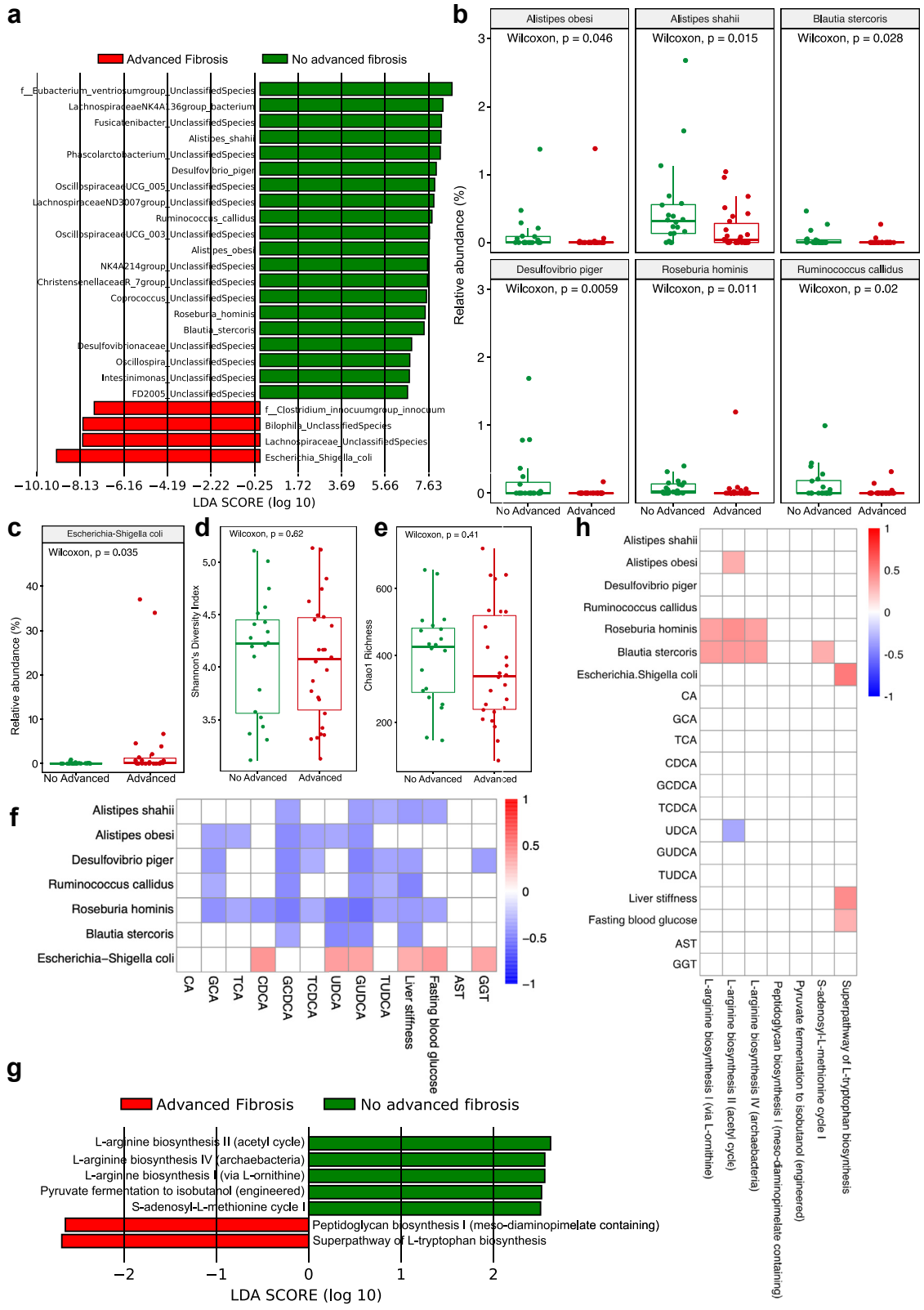
a
Advanced Fibrosis
No advanced fibrosis
f__Eubacterium_ventriosumgroup_UnclassifiedSpecies
LachnospiraceaeNK4A136group_bacterium
Fusicatenibacter_UnclassifiedSpecies
Alistipes_shahii
Phascolarctobacterium_UnclassifiedSpecies
Desulfovibrio_piger
OscillospiraceaeUCG_005_UnclassifiedSpecies
LachnospiraceaeND3007group_UnclassifiedSpecies
Ruminococcus_callidus
OscillospiraceaeUCG_003_UnclassifiedSpecies
Alistipes_obesi
NK4A214group_UnclassifiedSpecies
ChristensenellaceaeR_7group_UnclassifiedSpecies
Coprococcus_UnclassifiedSpecies
Roseburia_hominis
Blautia_stercoris
Desulfovibrionaceae_UnclassifiedSpecies
Oscillospira_UnclassifiedSpecies
Intestinimonas_UnclassifiedSpecies
FD2005_UnclassifiedSpecies
f__Clostridium_innocuumgroup_innocuum
Bilophila_UnclassifiedSpecies
Lachnospiraceae_UnclassifiedSpecies
Escherichia_Shigella_coli
−10.10 −8.13 −6.16 −4.19 −2.22 −0.25 1.72 3.69 5.66 7.63
LDA SCORE (log 10)
b
Alistipes obesi
Wilcoxon, p = 0.046
Alistipes shahii
Wilcoxon, p = 0.015
Blautia stercoris
Wilcoxon, p = 0.028
Desulfovibrio piger
Wilcoxon, p = 0.0059
Roseburia hominis
Wilcoxon, p = 0.011
Ruminococcus callidus
Wilcoxon, p = 0.02
Relative abundance (%)
No Advanced Advanced
c
Escherichia-Shigella coli
Wilcoxon, p = 0.035
Relative abundance (%)
No Advanced Advanced
d
Wilcoxon, p = 0.62
Shannon's Diversity Index
No Advanced Advanced
e
Wilcoxon, p = 0.41
Chao1 Richness
No Advanced Advanced
f
Alistipes shahii
Alistipes obesi
Desulfovibrio piger
Ruminococcus callidus
Roseburia hominis
Blautia stercoris
Escherichia−Shigella coli
CA GCA TCA CDCA GCDCA TCDCA UDCA GUDCA TUDCA Liver stiffness Fasting blood glucose AST GGT
1 0.5 0 −0.5 −1
h
Alistipes shahii
Alistipes obesi
Desulfovibrio piger
Ruminococcus callidus
Roseburia hominis
Blautia stercoris
Escherichia.Shigella coli
CA GCA TCA CDCA GCDCA TCDCA UDCA GUDCA TUDCA Liver stiffness Fasting blood glucose AST GGT
1 0.5 0 -0.5 -1
L-arginine biosynthesis I (via L-ornithine)
L-arginine biosynthesis II (acetyl cycle)
L-arginine biosynthesis IV (archaebacteria)
Peptidoglycan biosynthesis I (meso-diaminopimelate containing)
Pyruvate fermentation to isobutanol (engineered)
S-adenosyl-L-methionine cycle I
Superpathway of L-tryptophan biosynthesis
g
Advanced Fibrosis
No advanced fibrosis
L-arginine biosynthesis II (acetyl cycle)
L-arginine biosynthesis IV (archaebacteria)
L-arginine biosynthesis I (via L-ornithine)
Pyruvate fermentation to isobutanol (engineered)
S-adenosyl-L-methionine cycle I
Peptidoglycan biosynthesis I (meso-diaminopimelate containing)
Superpathway of L-tryptophan biosynthesis
−2 −1 0 1 2
LDA SCORE (log 10)

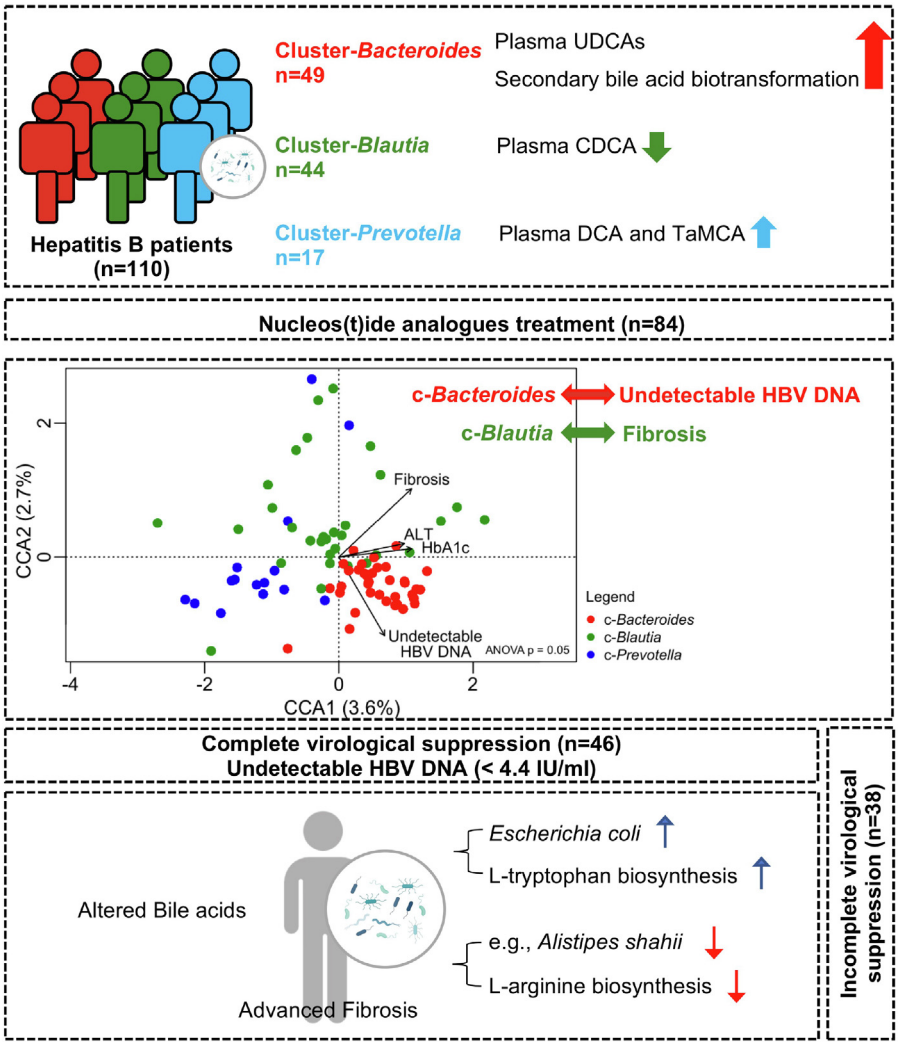


***Fig. 6:* Systemic diagram of the findings.** In the patients receiving nucleos(t)ide analogues therapy, the bacterial signature belonging to c-*Bacteroides* was associated with undetectable HBV DNA. HBV patients with advanced fibrosis had altered gut microbiota (increase in *Escherichia coli* but decrease in *Alistipes shahii*) and bile acid profiles compared with those without advanced fibrosis after successful virological control. *Escherichia coli* may play a role in HBV-related liver fibrosis after successful virological control. ALT, Alanine transaminase; CCA, canonical correspondence analysis; HbA1c, Glycated hemoglobin; UDCA, ursodeoxycholic acid; GLCA, glycolithocholic acid; CDCA, chenodeoxycholic acid; DCA, deoxycholic acid; TaMCA, tauro-α-muricholic acid.

patients without advanced fibrosis, had a higher discrimination ability (AUROC = 0.7087, p = 0.0162) when compared to *Escherichia coli* (AUROC = 0.6404, p = 0.1058, Table S8). L-arginine biosynthesis pathways were significantly increased in patients without advanced fibrosis and correlated positively with *Blautia stercoris* and *Roseburia hominis* (Fig. 5h). Furthermore, L-arginine has been shown to attenuate chronic liver fibrosis through the expression of endothelial nitric oxide synthase (eNOS).[41]

***Fig. 5:* The potential role of gut microbiome in HBV-related advanced fibrosis after successful virological control. (a)** Differentially abundant bacterial taxa between non-fibrosis and fibrosis in patients with undetectable HBV-DNA were determined by Linear discriminant analysis (LDA) Effect Size analysis. The results were plotted with a threshold of log LDA score greater than 3. **(b)** Proportion of downregulated signatures; **(c)** Proportion of upregulated signatures; **(d)** Shannon's diversity index and **(e)** Chao 1 richness of gut microbiota. **(f)** Heatmaps of the Spearman's rank correlation coefficient between differential species, clinical parameters, and differential BAs were filtered by |rho| > 0.3, p-value (adjusted by Benjamini-Hochberg) < 0.05. **(g)** Lefse method to identify the differential microbial pathways; **(h)** Heatmaps of the Spearman's rank correlation coefficient between differential pathways, clinical parameters, and differential BAs.

Thus, these two opposing pathways may be involved in the development of advanced fibrosis among NAs-treated CHB patients with undetectable HBV-DNA, and these pathways are linked to specific bacterial signatures. One is an increased abundance of *Escherichia coli* and its association with L-tryptophan biosynthesis pathway, and the other is linked to the decreased abundance of *Alistipes shahii, Alistipes obesi, Blautia stercoris, Desulfovibrio piger, Roseburia hominis, Ruminococcus callidus*.

In terms of limitations, the present study only recruited Chinese patients and was conducted in a single center. A small number of treatment-naïve patients were included in this cohort. Conducting verification cohorts involving multiple centers would help to further validate the role of gut microbiota in the response to antiviral treatment of HBV patients. In addition, as our study recruited patients during their liver transient elastography appointment, there was a skewed distribution of increased patients with F3/4 fibrosis (47.3%). While the fibrosis distribution may not be representative of a general chronic HBV cohort, it nonetheless facilitated meaningful comparative analysis between patients with and without advanced fibrosis. All recruited patients were HBeAg-negative; this was likely related to the median age of patients referred for transient elastography (61.2 years) and is reflective of the continued aging of the HBV-infected cohort in our locality.[51] Since the descriptive nature of our study may lack molecular mechanisms, future microbiological or biochemical studies to explore the molecular mechanisms and *in-vivo* interventional studies are required to enhance the translational potential of our research.

In conclusion, HBV patients in this study could be categorized into three clusters, which were dominated by *Bacteroides*, *Blautia*, and *Prevotella*. In the patients receiving nucleos(t)ide analogues therapy, the presence of *c-Bacteroides* was associated with a favorable HBV treatment response, suggesting that these bacteria may contribute to achieving an undetectable viral load. Distinct bile acid signatures (elevated UDCAs levels) found in c-*Bacteroides* could be attributed to the differential abundance in bacteria species corresponding to different secondary bile acid biotransformation pathways. The advanced fibrosis in on-treatment patients after successful virological control was also linked to microbial alterations (e.g., increased abundance of *Escherichia coli* and its association with L-tryptophan biosynthesis) and bile acid metabolism. The association between the gut microbiome and HBV treatment response sets up intriguing possibilities for optimizing HBV treatment.

#### Contributors

The authors declare that they have participated in the preparation of the manuscript and have seen and approved the final version.

S Zhang and HT Chau were involved in the study concept and design, acquisition of data, data analysis and interpretation, and drafting of manuscript. FY Huang and DK Wong were involved in the acquisition of laboratory measurements. HM Tun and LY Mak were involved in the acquisition of data. MF Yuen was involved in the study concept and design and critical revision of manuscript. WK Seto was involved in the study concept and design, securing research funding, analysis and interpretation of data, critical revision of manuscript, and overall study supervision.

#### Data sharing statement

All data, analysis protocols, and software packages related to the current study are present in the paper or supplementary materials. The raw sequencing data generated in this study has been deposited in the European Nucleotide Archive database (https://www.ebi.ac.uk/ena/browser/view/PRJEB64018) with the accession number PRJEB64018. We analyzed the sequences by following the well-known codes.

#### Declaration of interests

MF Yuen is an advisory board member and/or received research funding from AbbVie, Arbutus Biopharma, Assembly Biosciences, Bristol Myer Squibb, Dicerna Pharmaceuticals, GlaxoSmithKline, Gilead Sciences, Janssen, Merck Sharp and Dohme, Clear B Therapeutics, Springbank Pharmaceuticals; and received research funding from Arrowhead Pharmaceuticals, Fujirebio Incorporation and Sysmex Corporation. WK Seto received speaker's fees from AstraZeneca, is an advisory board member and received speaker's fees from Abbott, received research funding from Pfizer, Alexion Pharmaceuticals, Ribo Life Sciences, and Boehringer Ingelheim, and is an advisory board member, received speaker's fees and researching funding from Gilead Sciences. The remaining authors have no conflict of interest.

#### Acknowledgements

The authors thank Ms. Carol Chu for the patient recruitment, and to the Centre of PanorOmic Sciences, The University of Hong Kong for the 16S sequencing and targeted metabolomics.

#### Appendix A. Supplementary data

Supplementary data related to this article can be found at https://doi.org/10.1016/j.ebiom.2024.105101.

#### References

1 Betrapally NS, Gillevet PM, Bajaj JS. Gut microbiome and liver disease. *Transl Res*. 2017;179:49–59.
2 Abu-Shanab A, Quigley EM. The role of the gut microbiota in nonalcoholic fatty liver disease. *Nat Rev Gastroenterol Hepatol*. 2010;7:691–701.
3 Bajaj JS, Hylemon PB, Ridlon JM, et al. Colonic mucosal microbiome differs from stool microbiome in cirrhosis and hepatic encephalopathy and is linked to cognition and inflammation. *Am J Physiol Gastrointest Liver Physiol*. 2012;303:G675–G685.
4 Chen Y, Yang F, Lu H, et al. Characterization of fecal microbial communities in patients with liver cirrhosis. *Hepatology*. 2011;54:562–572.
5 Tripathi A, Debelius J, Brenner DA, et al. The gut–liver axis and the intersection with the microbiome. *Nat Rev Gastroenterol Hepatol*. 2018;15:397–411.
6 Yuen MF, Chen DS, Dusheiko GM, et al. Hepatitis B virus infection. *Nat Rev Dis Prim*. 2018;4:18035.
7 Wei X, Yan X, Zou D, et al. Abnormal fecal microbiota community and functions in patients with hepatitis B liver cirrhosis as revealed by a metagenomic approach. *BMC Gastroenterol*. 2013;13:1–8.
8 Ren Y-D, Ye Z-S, Yang L-Z, et al. Fecal microbiota transplantation induces hepatitis B virus e-antigen (HBeAg) clearance in patients with positive HBeAg after long-term antiviral therapy. *Hepatology*. 2017;65:1765–1768.
9 Chou H-H, Chien W-H, Wu L-L, et al. Age-related immune clearance of hepatitis B virus infection requires the establishment of gut microbiota. *Proc Natl Acad Sci*. 2015;112:2175–2180.
10 Gerard P. Metabolism of cholesterol and bile acids by the gut microbiota. *Pathogens*. 2013;3:14–24.
11 Caussy C, Hsu C, Singh S, et al. Serum bile acid patterns are associated with the presence of NAFLD in twins, and

dose-dependent changes with increase in fibrosis stage in patients with biopsy-proven NAFLD. *Aliment Pharmacol Therapeut*. 2019;49:183–193.
12 Jiao N, Baker SS, Chapa-Rodriguez A, et al. Suppressed hepatic bile acid signalling despite elevated production of primary and secondary bile acids in NAFLD. *Gut*. 2018;67:1881–1891.
13 Puri P, Daita K, Joyce A, et al. The presence and severity of nonalcoholic steatohepatitis is associated with specific changes in circulating bile acids. *Hepatology*. 2018;67:534–548.
14 Seto WK, Hui RWH, Mak LY, et al. Association between hepatic steatosis, measured by controlled attenuation parameter, and fibrosis burden in chronic hepatitis B. *Clin Gastroenterol Hepatol*. 2018;16:575–583 e2.
15 Yan H, Peng B, Liu Y, et al. Viral entry of hepatitis B and D viruses and bile salts transportation share common molecular determinants on sodium taurocholate cotransporting polypeptide. *J Virol*. 2014;88:3273–3284.
16 Wong VW, Petta S, Hiriart JB, et al. Validity criteria for the diagnosis of fatty liver by M probe-based controlled attenuation parameter. *J Hepatol*. 2017;67:577–584.
17 Karlas T, Petroff D, Sasso M, et al. Individual patient data meta-analysis of controlled attenuation parameter (CAP) technology for assessing steatosis. *J Hepatol*. 2017;66:1022–1030.
18 European Association for Study of L. Asociacion Latinoamericana para el Estudio del H. EASL-ALEH Clinical Practice Guidelines: non-invasive tests for evaluation of liver disease severity and prognosis. *J Hepatol*. 2015;63:237–264.
19 Callahan BJ, McMurdie PJ, Rosen MJ, et al. DADA2: high-resolution sample inference from Illumina amplicon data. *Nat Methods*. 2016;13:581–583.
20 Quast C, Pruesse E, Yilmaz P, et al. The SILVA ribosomal RNA gene database project: improved data processing and web-based tools. *Nucleic Acids Res*. 2012;41:D590–D596.
21 Arumugam M, Raes J, Pelletier E, et al. Enterotypes of the human gut microbiome. *Nature*. 2011;473:174–180.
22 Tun HM, Peng Y, Chen B, et al. Ethnicity associations with food sensitization are mediated by gut microbiota development in the first year of life. *Gastroenterology*. 2021;161:94–106.
23 Rousseeuw PJ. Silhouettes: a graphical aid to the interpretation and validation of cluster analysis. *J Comput Appl Math*. 1987;20:53–65.
24 Caliński T, Harabasz J. A dendrite method for cluster analysis. *Commun Stat Theor Methods*. 1974;3:1–27.
25 Milligan GW, Cooper MC. An examination of procedures for determining the number of clusters in a data set. *Psychometrika*. 1985;50:159–179.
26 ter Braak CJF. Canonical correspondence analysis: a new eigenvector technique for multivariate direct gradient analysis. *Ecology*. 1986;67:1167–1179.
27 Segata N, Izard J, Waldron L, et al. Metagenomic biomarker discovery and explanation. *Genome Biol*. 2011;12:1–18.
28 Song P, Zhang X, Feng W, et al. Biological synthesis of ursodeoxycholic acid. *Front Microbiol*. 2023;14:1140662.
29 Yan H, Zhong G, Xu G, et al. Sodium taurocholate cotransporting polypeptide is a functional receptor for human hepatitis B and D virus. *Elife*. 2012;1:e00049.
30 König A, Döring B, Mohr C, et al. Kinetics of the bile acid transporter and hepatitis B virus receptor Na+/taurocholate cotransporting polypeptide (NTCP) in hepatocytes. *J Hepatol*. 2014;61:867–875.
31 Lee HW, Park HJ, Jin B, et al. Effect of S267F variant of NTCP on the patients with chronic hepatitis B. *Sci Rep*. 2017;7:1–7.
32 Shen Y, Wu SD, Chen Y, et al. Alterations in gut microbiome and metabolomics in chronic hepatitis B infection-associated liver disease and their impact on peripheral immune response. *Gut Microb*. 2023;15:2155018.
33 Tan H, Zhai Q, Chen W. Investigations of Bacteroides spp. towards next-generation probiotics. *Food Res Int*. 2019;116:637–644.
34 Wang C, Zhao J, Zhang H, et al. Roles of intestinal bacteroides in human health and diseases. *Crit Rev Food Sci Nutr*. 2021;61:3518–3536.
35 Ramakrishna C, Kujawski M, Chu H, et al. Bacteroides fragilis polysaccharide A induces IL-10 secreting B and T cells that prevent viral encephalitis. *Nat Commun*. 2019;10:1–13.
36 Ogita T, Yamamoto Y, Mikami A, et al. Oral administration of flavonifractor plautii strongly suppresses Th2 immune responses in mice. *Front Immunol*. 2020;11:379.
37 Loomba R, Seguritan V, Li W, et al. Gut microbiome-based metagenomic signature for non-invasive detection of advanced fibrosis in human nonalcoholic fatty liver disease. *Cell Metabol*. 2019;30:607.
38 Shen B, Gu T, Shen Z, et al. Escherichia coli promotes endothelial to mesenchymal transformation of liver sinusoidal endothelial cells and exacerbates nonalcoholic fatty liver disease via its flagellin. *Cell Mol Gastroenterol Hepatol*. 2023;16:857–879.
39 Zhang Y, Jiang W, Xu J, et al. E. coli NF73-1 isolated from NASH patients aggravates NAFLD in mice by translocating into the liver and stimulating M1 polarization. *Front Cell Infect Microbiol*. 2020;10:535940.
40 Osawa Y, Kanamori H, Seki E, et al. L-tryptophan-mediated enhancement of susceptibility to nonalcoholic fatty liver disease is dependent on the mammalian target of rapamycin. *J Biol Chem*. 2011;286:34800–34808.
41 Leung TM, Tipoe GL, Liong EC, et al. Endothelial nitric oxide synthase is a critical factor in experimental liver fibrosis. *Int J Exp Pathol*. 2008;89:241–250.
42 Chen J, Vitetta L, Henson JD, et al. Intestinal dysbiosis, the tryptophan pathway and nonalcoholic steatohepatitis. *Int J Tryptophan Res*. 2022;15:11786469211070533.
43 Nocito A, Dahm F, Jochum W, et al. Serotonin mediates oxidative stress and mitochondrial toxicity in a murine model of nonalcoholic steatohepatitis. *Gastroenterology*. 2007;133:608–618.
44 Kwan SY, Jiao J, Qi J, et al. Bile acid changes associated with liver fibrosis and steatosis in the Mexican-American population of south Texas. *Hepatol Commun*. 2020;4:555–568.
45 Chen W, Ding M, Ji L, et al. Bile acids promote the development of HCC by activating inflammasome. *Hepatol Commun*. 2023;7.
46 Feng S, Xie X, Li J, et al. Bile acids induce liver fibrosis through the NLRP3 inflammasome pathway and the mechanism of FXR inhibition of NLRP3 activation. *Hepatol Int*. 2024. https://doi.org/10.1007/s12072-023-10610-0.
47 Zhang X, Coker OO, Chu ES, et al. Dietary cholesterol drives fatty liver-associated liver cancer by modulating gut microbiota and metabolites. *Gut*. 2021;70:761–774.
48 Parker BJ, Wearsch PA, Veloo ACM, et al. The genus Alistipes: gut bacteria with emerging implications to inflammation, cancer, and mental health. *Front Immunol*. 2020;11:906.
49 Shao L, Ling Z, Chen D, et al. Disorganized gut microbiome contributed to liver cirrhosis progression: a meta-omics-based study. *Front Microbiol*. 2018;9:3166.
50 Li J, Sung CY, Lee N, et al. Probiotics modulated gut microbiota suppresses hepatocellular carcinoma growth in mice. *Proc Natl Acad Sci U S A*. 2016;113:E1306–E1315.
51 Mak LY, Hui RW, Lee CH, et al. Glycemic burden and the risk of adverse hepatic outcomes in patients with chronic hepatitis B with type 2 diabetes. *Hepatology*. 2023;77:606–618.